11th International Symposium on Magnetic Bearings
August 26-29, Nara, Japan

SELF–SENSING OF NON–LAMINATED AXIAL MAGNETIC BEARINGS: MODELLING AND VALIDATION

Raoul Herzog, Sébastien Vuilloud
HEIG–VD, Haute Ecole d'Ingénierie et de Gestion du Canton de Vaud, Yverdon-les-Bains, 1401, Switzerland
raoul.herzog@heig-vd.ch

Roman Amstad, Gorka Galdos, Philippe Muellhaupt, Roland Longchamp
EPFL, Ecole Polytechnique Fédérale de Lausanne, Lausanne, 1015, Switzerland
philippe.muellhaupt@epfl.ch

ABSTRACT

The present paper proposes a refined nonlinear axial bearing model not too complex for real–time applications, which may potentially improve the estimator quality of modulation–based self–sensing.

Measurements show that the AC component (ripple) of the bearing current is an *underlinear* function of the AC excitation voltage, which causes the bearing admittance amplitude $|Y(j\omega, i_{ac})|$ to considerably increase at low amplitudes of i_{ac}. The non–consideration of this effect might explain the poor dynamic performance observed in former implementations of modulation–based self–sensing.

The model proposed in this paper includes a *dynamic* (rate dependent) hysteresis model of the Bertotti type, where the magnetic H field is a nonlinear function of the time derivative of flux density dB/dt. Eddy currents are modelled by a linear lumped RL ladder network (Cauer type). The proposed model gives encouraging results and is able to reproduce some of the observed phenomena.

INTRODUCTION

Self–sensing permits active magnetic bearings to dispense with dedicated position sensors and, instead, reconstruct rotor position information from the voltage and current signals of the actuator coils. Thus, the hardware amount in the machine environment and the amount of cabling can be reduced, which potentially increases hardware reliability.

Although self–sensing technology has progressed in terms of theoretical understanding [1, 2] and by the launching of commercial applications, some unsolved technical challenges impede the application of self–sensing to a broader range of applications. One of these technical challenges concerns self–sensing for non–laminated axial bearings. Non–laminated thrust bearings are a difficult candidate for self–sensing because of both the presence of strong eddy current effects and magnetic material nonlinearity.

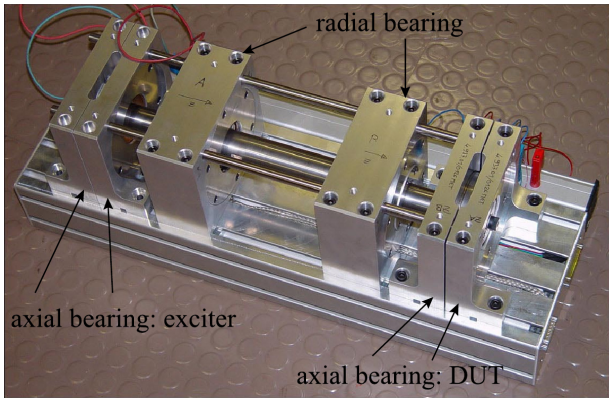

FIGURE 1: Magnetic Bearing Test Rig from MECOS.

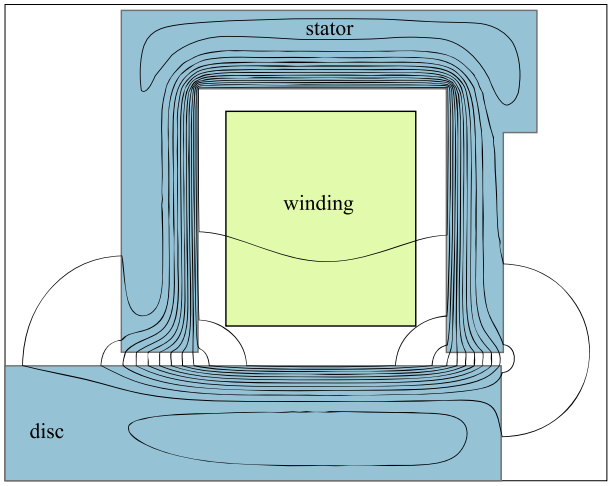

FIGURE 2: Flux density obtained by linear FEM simulation (COMSOL) @20 Hz, with $\mu_r = 5'000$ and $\sigma = 2 \cdot 10^6\ S/m$.

On the one hand the dynamics of axial bearings is simple because the rotor motion is essentially a rigid body motion decoupled from the radial displacements. On the other hand, the inductor dynamics of axial bearings is quite complicated because both stator and axial disc are usually non–laminated, which causes strong eddy currents. At high frequencies eddy currents mask the change of reluctance w.r.t. the gap, and therefore degrade gap sensitivity of actuator impedance.

The achievable performance of self–sensing heavily depends on the quality of the estimator model which is used for compensating all influencing factors like eddy currents and nonlinear magnetic material behaviour [3]. Therefore, the present paper focuses on modelling and validation of non–laminated axial bearings. The model should reflect both low–signal current ripple behaviour and high–signal load behaviour in both the low frequency range utilized for control (typical bandwidth <100 Hz), and the high frequency range used by the interrogation signal (typically >1 kHz).

Figure 2 shows the typical shielding effect caused by eddy currents already visible at 20 Hz. The field lines are more homogeneous in the air gap than in the stator. There is an interesting transition zone near the pole where the field lines abruptly change direction. Zhu [5] proposed a model where the magnetic circuit is decomposed in regions with analytical field solutions. The equivalent magnetic reluctances of the individual regions are combined. The elegant approach [5] is limited to linear material behaviour which is shown not to be suitable for the present problem.

AXIAL SELF–SENSING TEST RIG

Figure 1 shows the mechanical part of a highly versatile test rig built up with commercial electromechanical components from the magnetic bearing manufacturer MECOS Traxler AG. Two independent axial bearings are mounted on both ends of a horizontal rotor shaft.

One of the axial bearings is used as device under test (DUT) for self–sensing. The other one can be used optionally as an exciter for simulating external disturbance forces. This allows for better performance evaluation of self–sensing. Each axial bearing is differential with opposite stators mounted on movable housings which are screwed onto a support profile which allows to easily change the nominal air gap. The axial discs are also removable for testing different materials. The radial AMB's are just used to eliminate friction. The data of the axial DUT is given by table 1.

The following measurement equipment was used:

- impedancemeter HP4192A permitting to measure the small–signal harmonic impedance of the actuator coil at excitation levels < 1V (internal resistance 50Ω),
- linear power amplifier KEPCO BOP72-6M for analysing large–signal behaviour, driven by a
- GPIB programmable AC signal generator HP 33120A and a superposable DC bias signal source HP E3631A,
- 2–state PWM amplifier with variable supply voltage < 50V and variable switching frequency,
- current probes HP AM503, Agilent N2775A, and a differential voltage probe Acree SI9000,
- data acquisition board NI 6110 controlled by Matlab.

MEASUREMENTS

In this paper, the term *transfer function* is used in the sense of *description function*, i.e. the complex ratio "out/in" of the fundamental spectral components of input and output signals. All of the measurements show that higher order harmonics can be neglected. Figure 3 shows the behaviour of equivalent inductance $L_{eq} = \Im m(Z)/\omega$ w.r.t. excitation frequency and air gap. At frequencies above 1 kHz, the equivalent inductance is almost independent of the airgap. The equivalent resistance $\Re e(Z)$ keeps a usable airgap sensitivity up to ≈ 2 kHz, figure 4.

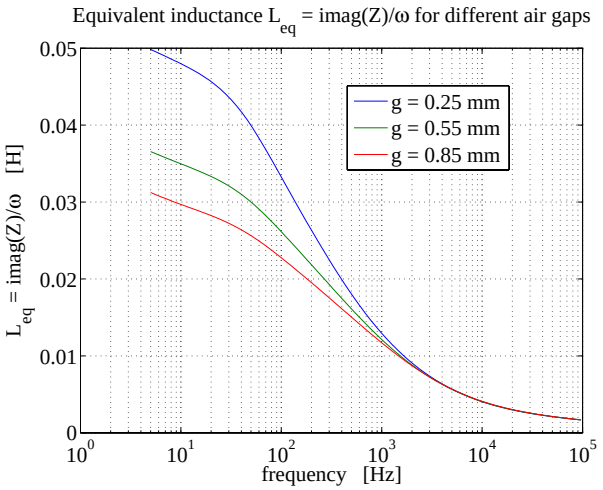

FIGURE 3: Inductance measurement with impedancemeter HP4192A @ 1V excitation level.

TABLE 1: axial bearing data

	symbol	value	unit
number of turns	N	180	-
max. current	I_{max}	3	A
max. PWM voltage	U_{max}	50	V
actuator force @ 3A and $g_0 = 0.55$ mm	F	150	N
inner diameter inner pole	d_{1i}	55.0	mm
outer diameter inner pole	d_{1o}	61.3	mm
inner diameter outer pole	d_{2i}	81.6	mm
outer diameter outer pole	d_{2o}	86.2	mm
nominal air gap	g_0	0.55	mm
axial clearance	Δg	± 0.3	mm
mean pole area	A_{fe}	589	mm^2
mean iron length (approx.)	l_{fe}	52	mm
winding section area	A_w	67.3	mm^2
stator material Böhler P822, not tempered	1.3842	Si 2.7	%
rotor disc material (ECN35)	1.5752	14NiCr14	-
coil resistance at DC	R_c	3.07	Ω
nominal inductance @ g_0=0.55 mm, 1Hz, I_{ac}=1.5A	$L_{0,nom}$	39	mH

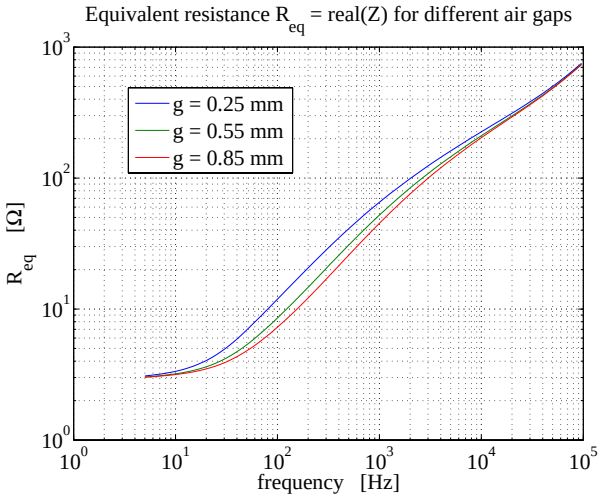

FIGURE 4: Resistance measurement with impedancemeter HP4192A @ 1V excitation level.

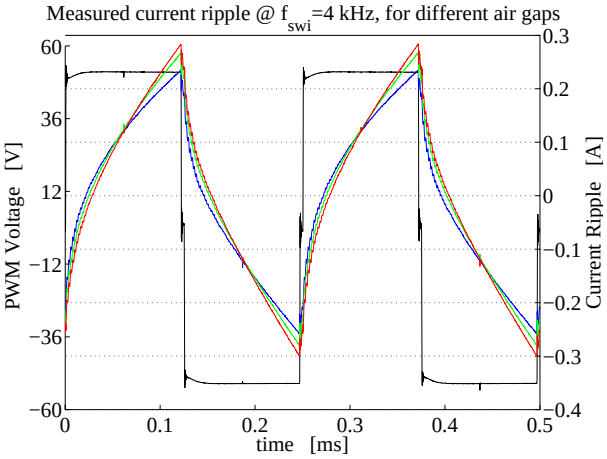

FIGURE 5: Current ripple measurement (blue: $g = 0.25$mm, green: $g = 0.55$mm, red: $g = 0.85$mm), with a 2-state PWM voltage of 50V, 4kHz, 50% duty cycle.

Figure 5 shows that the current ripple varies of ≈ 20% within the axial clearance in case of a 2–state 50V PWM amplifier with 4 kHz switching frequency and 50 % duty cycle.

A surprising result of the measurements was the appearance of a strong nonlinearity which behaves *contrary* to saturation, i.e. which influences at *low* amplitudes. Figure 6 shows that the bearing admittance amplitude $|Y(j\omega, i_{ac})|$ at a fixed frequency of 4 kHz is considerably increasing at low amplitudes of the sinusoidal excitation i_{ac}. This results in an *underlinear* behaviour: when the voltage doubles, the current will be *less* than the double. The waveform shape of the current remains almost sinusoidal, and harmonic distortion is small.

In the following modelling section a special emphasis is placed on reproducing this phenomenon.

MODELLING

Magnetic Material Modelling

It is impossible to model the observed amplitude dependency with a classical static B–H curve. Therefore, we focused on hysteresis, especially *dynamic* hysteresis. Literature about hysteresis modelling is abundant. For self–sensing purposes the magnetic

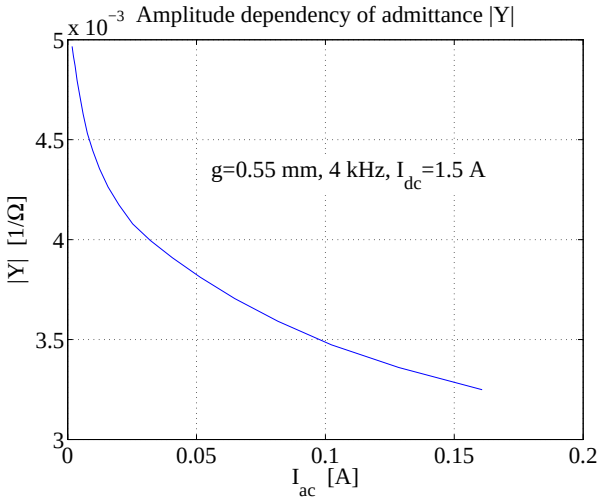

FIGURE 6: Measured admittance amplitude $|Y(u_{ac})|$ as a function of excitation amplitude.

material model should be simple enough for real–time implementation, and the number of parameters should not be too high. An appropriate model was proposed by Bertotti [6], who classified the ferromagnetic hysteresis effects into three components: static rate–independent hysteresis, rate–dependent linear eddy currents, and rate–dependent *nonlinear* excess eddy currents. The latter occur when the magnetic domain walls move. The resulting microscopical eddy currents create a counter field that has a dependency proportional to $\sqrt{dB/dt}$. Ribbenfjärd [7] modified the eddy current modelling of [6], in order to cope with magnetic materials thicker than the characteristic penetration depth δ,

$$d > \delta = \sqrt{\frac{1}{\pi\,\sigma\,\mu\,f}} \tag{1}$$

where d denotes the thickness, σ the electrical conductivity, μ the magnetic permeability, and f the applied frequency. The approach of Ribbenfjärd [7] consists of combining the excess eddy term of Bertotti with a lumped RL ladder network (Cauer type) discretizing the distributed eddy currents. This allows a more precise modelling of the shielding effect caused by eddy currents in thick materials.

The modelling in the present work follows the above idea. The magnetic material behaviour will be described by the following *phenomenological* model:

$$H_{fe}(B_{fe},\ \tfrac{dB_{fe}}{dt}) = H_{fe,stat}(B_{fe}) + b\left(\sqrt{1 + c\left|\tfrac{dB_{fe}}{dt}\right|} - 1\right)\operatorname{sign}(\tfrac{dB_{fe}}{dt}) \tag{2}$$

with

$$b = \frac{n_0\,V_0}{2} \tag{3}$$

$$c = \frac{4\,\sigma\,G\,d\,w}{n_0^2\,V_0}. \tag{4}$$

In (3) and (4), σ is the electrical conductivity, d is the thickness and w the material width. Furthermore, G is a parameter depending on the structure of magnetic domains, n_0 is a phenomenological parameter related to the number of active correlation regions when $f \to 0$, whereas V_0 determines how microstructural features like grain size, crystallographic textures, residual stresses, etc. affect the number of active correlation regions [6]. For simplicity, we will work directly with the two independent parameters b and c instead of working with the six physical/phenomenological parameters $n_0, V_0, \sigma, G, d, w$. Since static hysteresis is quite small in magnetic bearings, the first term $H_{fe,stat}(B_{fe})$ in (2) can be replaced by a *static memoryless* B–H curve with saturation. The second term in (2) corresponds to the Bertotti term for modelling *excess* eddy currents.

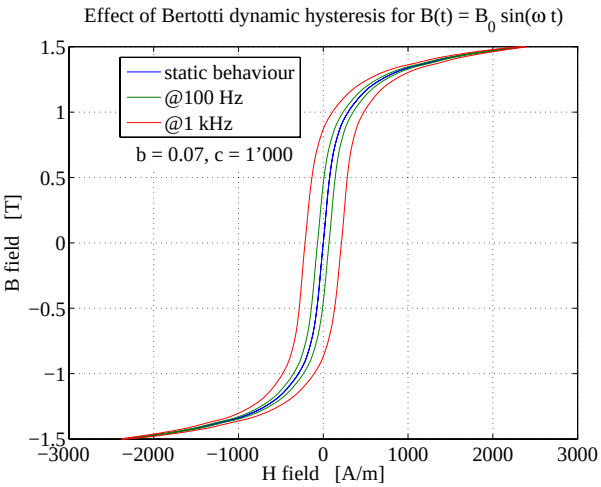

FIGURE 7: B–H diagram for harmonic excitation.

The effect of the Bertotti term is twofold. Firstly, the hysteresis curve is *widening up* at higher frequencies, thus causing higher losses, see figure 7. Secondly, the effect of the square root *increases* dH/dB for small signals, which corresponds to a *lower* value of incremental permeability, hence a lower bearing inductance.

Magnetic circuit modelling

By combining Faraday's and Ohm's law, input voltage u applied to the bearing magnet induces a magnetic flux Φ according to

$$u \;=\; R_c\, i \;+ N\,\frac{d\Phi}{dt} \tag{5}$$

where N denotes the number of turns, and R_c the ohmic resistance of the coil. The classical eddy currents will be modeled by a fictitious secondary 1–turn winding loaded by a RL ladder network. This leads to a state space representation of the following form

$$\frac{d\,\mathbf{i}_e}{dt} = \mathbf{A}_e\,\mathbf{i}_e + \mathbf{B}_e\frac{d\Phi}{dt} \tag{6}$$

$$i_{e,\mathrm{tot}} \;=\; \mathbf{C}_e\,\mathbf{i}_e \tag{7}$$

where the state variables are the currents in the network inductances. The state space matrix $\mathbf{A}_e$ of the ladder network is shown to be lower triangular

$$\mathbf{A}_e = \begin{bmatrix} -\frac{R_{e1}}{L_{e1}} & 0 & 0 & \cdots & 0 \\ -\frac{R_{e1}}{L_{e2}} & -\frac{R_{e2}}{L_{e2}} & 0 & \cdots & 0 \\ \vdots & \vdots & \ddots & 0 & 0 \\ \vdots & \vdots & \vdots & \ddots & 0 \\ -\frac{R_{e1}}{L_{ene}} & -\frac{R_{e2}}{L_{ene}} & -\frac{R_{e3}}{L_{ene}} & \cdots & -\frac{R_{ene}}{L_{ene}} \end{bmatrix} \tag{8}$$

n_e being the number of stages in the ladder network. The input and output matrices $\mathbf{B_e}$, $\mathbf{C_e}$ are given by

$$\mathbf{B}_e = \begin{bmatrix} \frac{1}{L_{e1}} \\ \frac{1}{L_{e2}} \\ \vdots \\ \frac{1}{L_{ene}} \end{bmatrix},\quad \mathbf{C}_e \;=\; \begin{bmatrix} 1 & 1 & \cdots & 1 \end{bmatrix} \tag{9}$$

Without the RL ladder network the current waveform $i(t)$ is almost triangular when excited with a PWM square wave $u(t)$. The presence of the ladder network introduces zeros and poles at high frequencies. These additional zeros and poles deform the current waveform $i(t)$ to feature cusps and to match figure 5. Instead of using time domain identification we preferred identification in the frequency domain. Using an iterative weighted Levy method based on least square, a 4th order black box identification of the global admittance transfer function has been carried out, which yields a good fit, figure 8. The measured bearing admittance $Y(j\omega)$ has a slope of $\approx -14\,\mathrm{dB/dec}$ in the Bode magnitude plot, figure 8, which reveals the *fractional order* nature of distributed eddy currents. The identification yields an approximating 4th order rational transfer function featuring interlacing poles and zeros on the real axis. By applying continued fraction expansion the corresponding physical parameters R_i, L_i associated to the RL ladder network have been calculated.

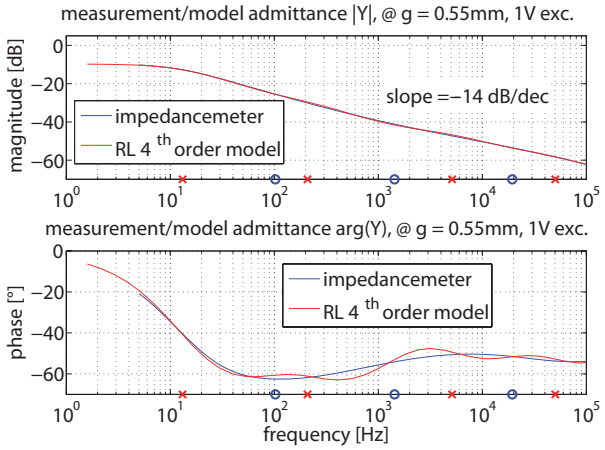

FIGURE 8: Bode diagram of measured admittance $Y = 1/Z$, the least square fitting of a 4th order RL ladder type model, and its pole/zero constellation $\times$ $\circ$.

The application of Ampère's law, and the hypothesis of homogeneous field distribution leads to

$$N\,i - i_{e,tot} \;=\; \frac{2\,g}{\mu_0\,A}\Phi + l_{fe}\,H_{fe}(B_{fe},\;\frac{dB_{fe}}{dt}) \tag{10}$$

Eliminating the algebraic loop

When combining (2), (5) and (10), and choosing $B_{fe} = \Phi/A_{fe}$ as variable, an algebraic loop in dB_{fe}/dt occurs, because a change in dB_{fe}/dt directly changes H_{fe} via the Bertotti excess term, which influences the current i via Ampère's law, which in turn changes again dB_{fe}/dt. In order to avoid potential numerical problems and to reduce calculation time, we eliminated the algebraic loop by some algebraic manipulations. By eliminating i from (10), (5) becomes

$$f(\tfrac{d\,B_{fe}}{dt}) \;=$$

$$\tfrac{u}{N\,A} - \tfrac{2\,R_c\,g}{\mu_0 N^2 A}B_{fe} - \tfrac{R_c}{N^2 A}i_{e,tot} - \tfrac{R_c\,l_{fe}}{N^2 A}H_{fe,stat}(B_{fe}) \tag{11}$$

with

$$f(x) = x + \tilde{b}\left(\sqrt{1 + c\,|x|} - 1\right)\,\mathrm{sign}\,(x) \quad (12)$$

$$\tilde{b} = \frac{R_c\, l_{fe}}{N^2\, A_{fe}}\, b \quad (13)$$

The inverse function of $f(x)$ is $g(f(x)) = x$ with

$$g(x) = \frac{2\,(\tilde{b} + |x|) + \tilde{b}^2 c - \tilde{b}\sqrt{(2 + \tilde{b}c)^2 + 4c|x|}}{2}\,\mathrm{sign}\,(x) \quad (14)$$

The resulting differential equation with eliminated algebraic loop becomes

$$\frac{d\,B_{fe}}{dt} = g\left(\frac{u}{NA} - \frac{2\,R_c\,g}{\mu_0 N^2 A} B_{fe} - \frac{R_c}{N^2 A} i_{e,tot} - \frac{R_c\, l_{fe}}{N^2 A} H_{fe,stat}(B_{fe})\right) \quad (15)$$

The Bertotti term introduces a *nonlinear feedthrough* term from input voltage u to output current i because dB/dt appears in the output equation (10). Therefore, the Bertotti term contributes to the current cusps in case of PWM voltage supply.

Modelling fringing and leakage effects

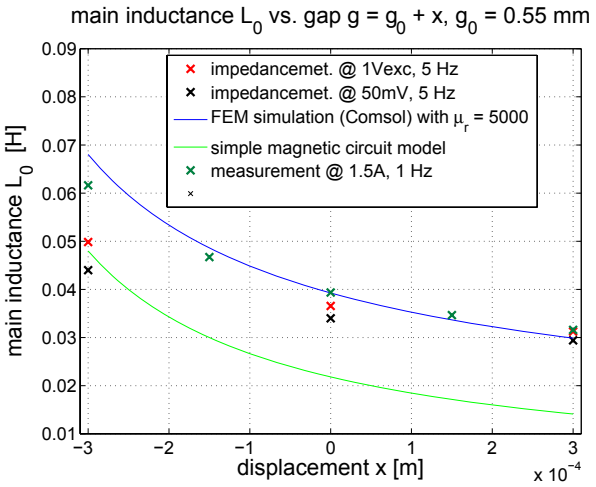

FIGURE 9: Main inductance $L_0(g)$ at very low frequencies, $L_0(g) = \lim_{\omega\to 0} \Im m(Z,g)/\omega$.

Figure 9 shows the measured and simulated main inductance $L_0(g) = \lim_{\omega\to 0} \Im m(Z,g)/\omega$ as a function of air gap g. The eddy currents are neglectable at low frequencies, and the contribution of the Bertotti term is also small. The measurements are still amplitude dependent. Additionally, the simple magnetic circuit based on a theoretical airgap reluctance $R_m = 2\,g/(\mu_0\, A_{fe})$ gives too low values for inductance $L_0(g)$. Fringing effects lead the magnetic field to occupy more space than just iron area A_{fe}. Increasing the "effective" air gap area by a constant factor does not give satisfying results. Instead, a simple gap-dependent equivalent area $A_{eq}(g) = A_0\,(1 + k_g\, g)$ permits to match the measured values of $L_0(g)$.

RESULTS AND CONCLUSION

A global Simulink model of the axial bearing has been built with input signal $u(t)$ and output signal $i(t)$. This model incorporates three *nonlinear* blocks: the static nonlinear B–H curve, the Bertotti excess eddy current term, and the inverse function g which serves to eliminate the algebraic loop. Furthermore, the Simulink model features a state–space block for modelling the ladder network (8), (9). This allows to change the number of RL stages without modifying the Simulink model. Three eddy current RL stages were found to be sufficient for a good fit in the frequency range $0\ldots 20$kHz. Thus, the order of the global system is 4 with the state variables Φ, i_{e1}, i_{e2}, and i_{e3}. The parameters used for simulation are given by table 2. These parameters are approximative and not yet optimized. Figure 10 shows the result of the simulated admittance amplitude $|Y(i_{ac})|$. For each value of the excitation amplitude, the Simulink simulation was started with approximative initial values. The simulation was run until it converged sufficiently close to the periodic solution. Then a Fourier analysis of $i(t)$ was carried out, and the admittance $Y(i_{ac})$ was calculated as complex ratio of the fundamental components of current by voltage. Figure 10 demonstrates that the Simulink model qualitatively reproduces the measured amplitude dependency.

OUTLOOK

There remain a certain number of open questions. A first question concerns the choice of ferromagnetic material: instead of modelling and compensating complicated nonlinearities studied in this paper, one might also try to utilize "better" magnetic materials and/or optimize thermal treatment. This is certainly possible for the axial stator when cost is not critical, but the severe mechanical requirements for the rotating disc reduce the number of alternative solutions.

There remain some questions about modelling, e.g. why attributing *all* of the Bertotti type nonlinearity only to the "main magnetic circuit", and not also

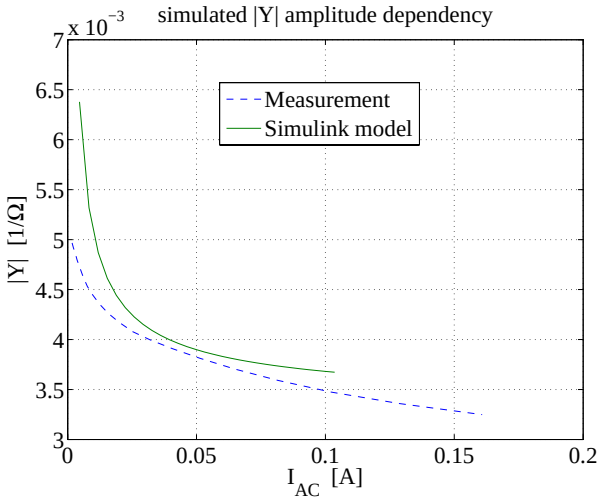

FIGURE 10: Mesured and simulated admittance amplitude $|Y(i_{ac})|$ as a function of excitation amplitude i_{ac} @ 4 kHz, $g = 0.55$mm.

TABLE 2: model data

	symbol	value	unit
Bertotti term b	b	0.14	A/m
Bertotti term c	c	1'000	s/Tesla
fringing correction term A_0	A_0	537	mm^2
fringing correction term k_g	k_g	1.73	1/mm
eddy inductance L_1	L_1	2.51	μH
eddy inductance L_2	L_2	0.49	μH
eddy inductance L_3	L_3	0.23	μH
eddy resistance R_1	R_1	3.8	mΩ
eddy resistance R_2	R_2	16.6	mΩ
eddy resistance R_3	R_3	74.1	mΩ

to the eddy current network? This certainly needs further investigation.

The parameter identification needs a better strategy. There are too many parameters and too many measurement conditions for a common nonlinear optimization search algorithm. A clever identification sequence might decouple the optimization problem in a series of smaller ones.

A next question concerns the choice of frequency for the dither signal (PWM or separate interrogation signal). Figure 3 shows that sensitivity improves considerably at low frequencies. Rotor vibration caused by the interrogation signal could be canceled by the opposite bearing setup (e.g. bias excitation). Is a time scale separation between control signals and interrogation signal really necessary?

Finally, the proposed modelling must be incorporated and tested in a self-sensing estimation scheme. Extended Kalman estimators might be an alternative to the formal parameter estimation scheme proposed in [2].

Even though research in self–sensing AMB has been done for 20 years now, there still remain some challenging questions.

REFERENCES

1. Maslen E., Self–sensing for Active Magnetic Bearings: Overview and Status, Proc. of the 10th Int. Symp. on Magnetic Bearings, Martigny, Switzerland, Aug. 2006.

2. Maslen E., Iwasaki T., and Mahmoodian R., Formal Parameter Estimation for Self–sensing, Proc. of the 10th Int. Symp. on Magnetic Bearings, Martigny, Switzerland, Aug. 2006.

3. Schammass A., Herzog R., Bühler Ph., and Bleuler H., New Results for Self–Sensing Active Magnetic Bearings using Modulation Approach, IEEE transactions on Control Systems Technology, p. 509-516, Vol. 13, No. 4, July 2005.

4. Springer H., Schlager G., Platter T., A Nonlinear Simulation Model for Active Magnetic Bearing Actuators, Proc. of the 6th Int. Symp. on Magnetic Bearings, MIT Cambridge, USA, Aug. 5-7 1998.

5. Zhu L., Non-Laminated Magnetic Actuators for Magnetic Levitation, dissertation, University of Virginia, USA, Feb. 2005

6. Bertotti G., Hysteresis in Magnetism, Academic Press, Inc., pp 391-430, 1998.

7. Ribbenfjärd D., Engdahl G., Novel Method for Modeling of Dynamic Hysteresis, Proc. of Compumag 2007.

8. Ribbenfjärd D., Engdahl G., Modeling of Dynamic Hysteresis with Bergqvist's Lag Model, IEEE trans. on Magnetics, vol. 42, no. 10, Oct. 2006.